References

[1] J. Huang and J. A. Encinar, *Reflectarray Antennas*. Hoboken, NJ, USA: Wiley/IEEE Press, Nov. 2007, ISBN: 978-0-470-08491-5.

[2] J. A. Encinar *et al.*, "Dual-polarization dual-coverage reflectarray for space applications," *IEEE Trans. Antennas Propag.*, vol. 54, no. 10. pp. 2827–2836, Oct. 2006.

[3] T. Toyoda, D. Higashi, H. Deguchi, and M. Tsuji, "Broadband reflectarray with convex strip elements for dual-polarization use," in *Proc. Int. Symp. Electromag. Theory (EMTS'13)*, Hiroshima, Japan, May 20–24, 2013, pp. 683–686.

[4] R. E. Hodges and M. Zawadzki, "Design of a large dual polarized Ku band reflectarray for space borne radar altimeter," in *Proc. IEEE Antennas Propag. Soc. Int. Symp.*, Monterey, CA, USA, 2004, vol. 4, pp. 4356–4359.

[5] A. E. Martynyuk and J. I. Martinez Lopez, "Reflective antenna arrays based on shorted ring slots," in *Proc. IEEE Microw. Symp. Dig.*, Phoenix, AZ, USA, May 2001, vol. 2, pp. 1379–1382.

[6] A. Yu, F. Yang, A. Z. Elsherbeni, and J. Huang, "An X-band circularly polarized reflectarray using split square ring elements and the modified element rotation technique," in *Proc. IEEE Antennas Propag. Soc. Int. Symp.*, San Diego, CA, USA, Jul. 2008, pp. 1–4.

[7] S. Malfajani and Z. Atlasbaf, "Design and implementation of a broadband single layer circularly polarized reflectarray antenna," *IEEE Antennas Wireless Propag. Lett.*, vol. 11, pp. 973–976, Aug. 2012.

[8] B. Strassner, C. Han, and K. Chang, "Circularly polarized reflectarray with microstrip ring elements having variable rotation angles," *IEEE Trans. Antennas Propag.*, vol. 52, no. 4, pp. 1122–1125, Apr. 2004.

[9] C. Han, C. Rodenbeck, J. Huang, and K. Chang, "A C/Ka dual frequency dual layer circularly polarized reflectarray antenna with microstrip ring elements," *IEEE Trans. Antennas Propag.*, vol. 52, no. 11, pp. 2871–2876, Nov. 2004.

[10] J. Huang, C. Han, and K. Chang, "A Cassegrain offset-fed dual-band reflectarray," in *Proc. IEEE Antennas Propag. Soc. Int. Symp.*, Albuquerque, NM, USA, Jul. 2006, pp. 2439–2442.

[11] A. Yu, F. Yang, A. Z. Elsherbeni, and J. Huang, "Experimental demonstration of a single layer tri-band circularly polarized reflectarray," in *Proc. IEEE Antennas Propag. Soc. Int. Symp.*, Toronto, Canada, Jul. 11–17, 2010, pp. 1–4.

[12] C. Guclu, J. Perruisseau-Carrier, and O. A. Civi, "Proof of concept of a dual-band circularly-polarized RF MEMS beam-switching reflectarray," *IEEE Trans. Antennas Propag.*, vol. 60, no. 11, pp. 5451–5455, Nov. 2012.

[13] J. Huang and R. J. Pogorzelski, "A Ka-band microstrip reflectarray with elements having variable rotation angles," *IEEE Trans. Antennas Propag.*, vol. 46, no. 5, pp. 650–656, May 1998.

[14] S. Mener, R. Gillard, R. Sauleau, A. Bellion, and P. Potier, "Unit-cell for dual-circular polarisation reflectarrays," in *Proc. 8th Eur. Conf. Antennas Propag.*, The Hague, The Netherlands, Apr. 6–11, 2014, pp. 1615–1618.

[15] E. Girard, R. Moulinet, R. Gillard, and H. Legay, "An FDTD optimization of a circularly polarized reflectarray unit-cell," in *Proc. IEEE Antennas Propag. Soc. Int. Symp.*, San Antonio, TX, USA, Jun. 2002, vol. 3, pp. 136–139.

[16] S. Mener, R. Gillard, R. Sauleau, C. Cheymol, and P. Potier, "Design and characterization of a CPSS-based unit-cell for circularly-polarized reflectarray applications," *IEEE Trans. Antennas Propag.*, vol. 61, no. 4, pp. 2313–2318, Apr. 2013.

[17] R. Pereira, R. Gillard, R. Sauleau, T. Dousset, and X. Delestre, "Dual linearly-polarized unit-cells with nearly 2-bit resolution for reflectarray applications in X-band," *IEEE Trans. Antennas Propag.*, vol. 60, no. 12, pp. 6042–6048, Dec. 2012.

[18] S. Mener, R. Gillard, R. Sauleau, C. Cheymol, and P. Potier, "An improved topology for reconfigurable CPSS-based reflectarray cell," in *Proc. Eur. Conf. Antennas Propag. (EuCAP)*, Gothenburg, Sweden, Apr. 8–12, 2013, pp. 2721–2725.

Sidelobe Canceling for Reconfigurable Holographic Metamaterial Antenna

Mikala C. Johnson, Steven L. Brunton, Nathan B. Kundtz, and J. Nathan Kutz

Abstract—Accurate and efficient methods for beam-steering of holographic metamaterial antennas is of critical importance for enabling consumer usage of satellite data capacities. We develop an algorithm capable of optimizing the beam pattern of the holographic antenna through software, reconfigurable controls. Our method provides an effective technique for antenna pattern optimization for a holographic antenna, which significantly suppresses sidelobes. The efficacy of the algorithm is demonstrated both on a computational model of the antenna and experimentally. Due to their exceptional portability, low-power consumption, and lack of moving parts, holographic antennas are an attractive and viable technology when combined with proven software-based strategies to optimize performance.

Index Terms—Holography, satellite antennas, sidelobe canceling.

I. Introduction

The reconfigurable holographic metamaterial surface antenna (MSA) is an emerging technology for satellite communications. The MSA is a low-power device that is flat, thin, and lightweight. Moreover, it achieves active electronic scanning without any mechanical moving parts. However, in order to operate across its entire dynamic-scanning range, the antenna must be able to scan reliably without unacceptable levels of far-field radiation in undesired directions (sidelobes). It is therefore mandatory to suppress the production of sidelobes in a robust fashion while still preserving a strong main beam. We develop an optimization algorithm for the far-field pattern of an MSA that addresses these issues. Specifically, we demonstrate an algorithm for sidelobe suppression in software without resorting to nonadaptive hardware modifications.

Hardware developments for MSAs have recently undergone major innovations [1]–[3]. These works demonstrate the viability of building a metamaterial Ka-band antenna using existing materials and processes. However, the hardware antenna is only part of the system needed as the antenna also must have software control algorithms to achieve optimal beam performance, being able to tailor, in a rapid and robust fashion, the radiation pattern of the antenna to achieve the desired characteristics that include a high peak gain, acceptable beamwidth, and sidelobe suppression.

In this paper, we address the problem of sidelobe suppression for a holographic antenna. Section II covers the background for classical antenna sidelobe cancelation and holographic antennas. Section III describes the antenna system and computational model used to predict the behavior of the antenna investigated in this work. Section IV presents the algorithm developed for sidelobe reduction. Finally, in Section V, results demonstrating the efficacy of the algorithm on both the computational model and on experimental hardware are exhibited.

We then conclude the paper with discussion of the possibilities that our proposed control strategy provides.

II. BACKGROUND

A. Sidelobe Cancelation in Arrays

Sidelobe cancelation has a rich history in the academic literature as well as in practice. Several patents were issued for device configurations for sidelobe cancelation in the mid-1960 s [4]–[7]. Additionally, there are many previous works in sidelobe cancelation of digital beamforming networks [8]–[10].

However, unlike the operating principles of the metamaterial antenna, these early works dictate the use of spatially separate arrays and assume that the signal from each antenna comprising the array is separable, i.e., each element of the beamformer has its own transceiver chain consisting of amplifier, filter, mixer, etc. During the processing of the signal from each individual receiver, the interference signal is subtracted from the reference, and thus the unwanted information received from sidelobes is suppressed, an approach due to Widrow [11].

The holographic antenna, on the other hand, is engineered to treat the pattern and the control of the antenna in aggregate. The problem of sidelobe cancelation via software control under this condition has not, to the best of the authors' knowledge, been considered. In this work, we develop and demonstrate an effective extension of Widrow's cancelation technique to the holographic antenna.

B. Holographic Antennas

A microwave holographic antenna was first demonstrated by Checcacci, Russo, and Scheggi in 1970 [12]. Particularly interesting in their work, in light of the aims of the present work, is that their first interest beyond creating a beam-forming antenna was to reduce the "zeroth order" aberrations in the holographic image. They do not call these aberrations sidelobes, although that is what they are. They understood these aberrations to be errors in the holographic recording and addressed them accordingly by varying the approximation (pixelation and quantization) of the holographic recording to reduce this zeroth order.

Holographic antennas have been under development more intensely since the early 2000s since new materials better suited to the recording of RF holograms have been increasingly available. There have been several disparate approaches to realizing efficient holographic antennas, these include static artificial impedance surfaces [13]–[15], passive leaky-wave holographic antennas [16] (and the references therein), reconfigurable artificial impedance surfaces [17]–[20], and reconfigurable metamaterial antennas [21], [22] (the technology for which we develop our sidelobe reduction method). This literature on holographic antennas, heretofore, focuses on designing and improving the hardware devices that can accomplish the recording and illumination of a microwave hologram; these works do not consider optimization of the beam in control. We specifically address optimization of the reproduced holographic image in software control in the presence of the hardware limitations.

III. ANTENNA ARCHITECTURE AND BASIC CONTROL

A. Metamaterial Antenna

The MSA technology architecture is composed of a planar array of thousands of discrete, voltage-tunable meta-atoms (equivalently, unit cells, resonant cells, or resonators) packed closely together in a rectangular array and fed by the TE_{10} mode wave propagating in a rectangular waveguide beneath the elements [see Fig. 1(a)]. This structure leads to several characteristics that must be considered when approaching optimization of the radiation pattern.

First, a metamaterial antenna capable of closing a link with a satellite must have enough surface area to attain high enough gain. To achieve this basic performance requirement, the antenna is of the approximate dimensions shown in Fig. 1(a), and thus is composed of more than 10 000 continuously and individually controlled unit cells. The control of each cell varies the amplitude of scatter of the cell from a minimally excited state to a maximally excited state as the voltage tunes the resonant frequency of the cell. It is impractical and infeasible to try random controls, e.g., a genetic algorithm, in search of good control patterns.

Apart from the large number of cells, each meta-atom resonant cell responds nonlinearly in both phase and amplitude to its control. The cells do not display *independent* amplitude and phase modulation as a phased array would, but instead the amplitude and phase shift occur simultaneously as the control is changed. This resonant behavior is sensitive to manufacturing tolerances.

The coupling between the elements and the coupling between all the elements simultaneously with the underlying guided feed wave further complicates control. All elements are *simultaneously* slightly changing the feed wave based upon the applied controls. We refer the reader to [23] for more detailed analysis of the types of nonlinear coupling in this antenna system.

A circuit-schematic description of these complex coupled physics of the array is shown in Fig. 1(c). This image shows the traveling feed wave and the cells coupled to the waveguide. It also indicates the phase-shift from the underlying carrier phase due to the resonance of the cells.

A discrete dipole approximation-based model (DDA model) of the metamaterial antenna captures the effects mentioned above and has been demonstrated to more accurately predict the far-field radiation pattern of the antenna than other, simpler models typically used in metamaterial modeling, while being fast enough for algorithm experimentation and development [23]. The discrete-dipole approximation discretizes and solves the Maxwell field equations by assuming that each meta-atom is replaced by a dipole with a single complex polarizability (the polarizability of the cell being dependent on the controlled state of the resonator). The simultaneous interaction of the fields of all the approximate dipoles among themselves and with the feed wave is solved for, and the resulting dipole polarizations are used to predict the far-field pattern of the array. Refer to [23] for further details on the advantages, properties, and parameters of this model.

In this work, we use a DDA model of the metamaterial antenna of the type described in this section to develop and demonstrate our beam pattern optimization algorithm. The DDA model enables us to accurately predict the characteristic beam patterns of an ideal (manufacturing error-free) antenna. The ability to predict the characteristic patterns and the affect of changes in the control patterns allow us to use the model for the development of algorithms to improve the beam performance. However, it is not possible to take the control signals produced by the algorithm on a simulated antenna and transplant them to a fabricated antenna. The real world processes of building and controlling the antenna introduce enough variations that simple translation of patterns is suboptimal. Yet, the algorithm to improve the pattern, which permits the antenna to improve itself, *is* directly translatable between simulation and practice. The accuracy levels of both the DDA model and fabricated antennas enable us to design algorithms, but do not enable us to optimize control signals purely in simulation, as yet.
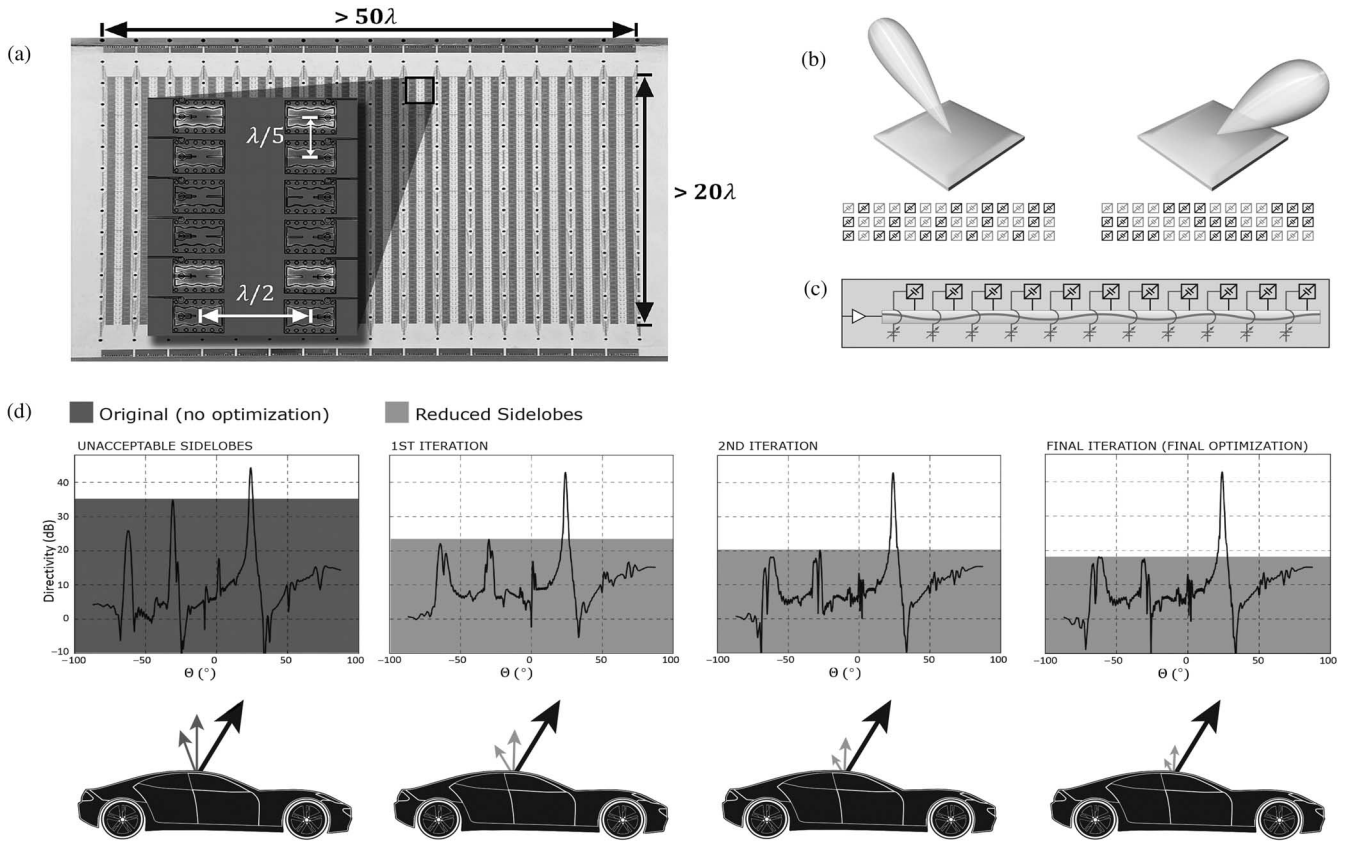
Fig. 1. (a) Example design of the reconfigurable holographic metamaterial antenna (RHMA) with exemplar dimensions and a close-up view of a small number of the arrayed tunable, meta-atoms (b) Holographic images on the surface of the array, when illuminated by an underlying feed wave, produce a coherent beam. Different images, encoded in the array by the control applied to each meta-atom, produce beams in different directions. (c) The physics of the metamaterial antenna. The input carrier wave traverses the waveguide, and the meta-atom cells couple energy out of the feed. Further, the cells produce simultaneous amplitude and phase-shift as a function of their control. (d) (top row) Simulated far-field results of the algorithm iteratively targeting different sidelobes while continuously creating a main beam in the direction of $25.7°$ θ. (bottom row) Representation of the simulated results in a mobile application, which is a technological goal of the RHMA system.

B. Holographic Control Theory

Here, we describe basic beamforming control strategy from a holography viewpoint upon which the optimization algorithm builds. The theory of holography is to encode on a surface (in this case, the antenna) an image such that when the surface is illuminated by a specified reference wave, the viewer sees a complete version of the originally recorded image in 3-D space.

In the case of an MSA, the desired 3-D image is a spherical wave emitted by (or converging upon) a point source in the far-field (the satellite). This propagating wavefront appears as a plane-wave on the flat surface of the antenna on earth. The illuminating reference wave is the wave that lights up the meta-atom resonators, the propagating electric-field in the waveguide

$$\Psi_{\mathrm{obj}}(\mathbf{r}; \theta_0, \phi_0) = \exp(-i\mathbf{k}_f(\theta_0, \phi_0) \cdot \mathbf{r}) \quad (1)$$
$$\Psi_{\mathrm{ref}}(\mathbf{r}) \approx \exp(-i\mathbf{k}_s \cdot \mathbf{r}) \quad (2)$$

where Ψ_{obj} is the desired far-field wave and Ψ_{ref} is the illuminating wave in the waveguide. $\mathbf{k}_f(\theta_0, \phi_0)$ is the desired directional complex propagation vector in free space, $\mathbf{k}_s$ is the complex propagation vector of the reference wave. In particular, we are interested in coordinates $\mathbf{r}$ that are on the surface of the antenna.

Note that (2) assumes that the illumination is from an ideal traveling wave within the waveguide; it assumes that the control pattern does not change this propagation (nor does anything else) and that there is

no phase shift between the underlying traveling wave and the radiated energy due to the resonant behavior of the cells. Both of these assumptions are false, but provide a useful approximation. In fact, the above assumption is accurate enough to ensure that the main beam points in the intended direction. The problem is the resolution of the rest of the pattern, i.e., the unintended sidelobes induced by the inaccuracy.

The interference of the object and reference wave is defined by

$$\Psi_{\mathrm{int}f} =: \Psi_{obj}\Psi_{ref}^*. \quad (3)$$

This interference pattern is recorded on the antenna by controlling the properties of the individual meta-atoms, such that when the interference pattern is lit up by the original reference wave, we obtain

$$\Psi_{\mathrm{int}f}\Psi_{\mathrm{ref}} \propto \Psi_{\mathrm{obj}}|\Psi_{\mathrm{ref}}|^2. \quad (4)$$

That is, the result has an amplitude proportional to the input wave, and it points in the direction of the object beam.

To record the image, we take the strategy of turning on cells where the reference wave displays the correct phase of the object wave and turning off cells where the reference wave displays an incorrect phase. This strategy is parameterized mathematically by

$$m(\mathbf{r}_n; \theta_0) = \frac{\Re(\Psi_{\mathrm{int}f}) + 1}{2} \quad (5)$$

where $\Re(\Psi_{\mathrm{int}f})$ indicates the real part of the complex interference pattern.

This resulting real-valued control is a shifted and scaled cosine wave, $\cos((\mathbf{k}_s - \mathbf{k}_f(\theta_0, \phi_0)) \cdot \mathbf{r})$. A depiction of sinusoidal control patterns producing different beams is shown in Fig. 1(b). Control patterns of different length period produce different beams. According to the parameterization, 1 corresponds to tuning a cell to a state of maximal scatter while 0 corresponds to a state of minimal scatter, and a value in between $(0, 1)$ linearly corresponds to a proportional amount of scatter between minimal and maximal.

Sidelobes may be produced by a myriad of causes including the distance between elements, the finite array size, and errors in the reference wave due to the application of the controls. Yet, from many computational experiments and from measurement of devices, we have found that the largest sidelobes come from harmonics in the cosine wave control induced by the phase-shifting effect of the resonant elements; the Discrete Fourier transform of the sampled modulation pattern shows a large spike in the Fourier frequency associated with the desired far-field pointing angle, but also higher order harmonic content as well. The algorithm presented next is especially useful for these harmonic lobes, though it can be effective for some other types of sidelobes as well.

IV. ALGORITHM

The sidelobe targeting algorithm starts from the control strategy that was derived in Section III-B and is given in (5), step 1 in Fig. 2.

The initial control pattern for an array scanning to the angle θ_0, ϕ_0 is

$$m(\mathbf{r}_n; \theta_0, \phi_0) = \frac{\cos((\mathbf{k}_s - \mathbf{k}_f(\theta_0, \phi_0)) \cdot \mathbf{r}_n) + 1}{2}. \quad (6)$$

The algorithm to reduce particularly high-energy sidelobes destructively interferes a second "main beam" with the targeted sidelobe. In control, it amounts to mangling the original single-tone cosine wave by superimposing the auxiliary control pattern to produce the image of the sidelobe upon it. The effect will be a two-toned (or multitoned if more than one sidelobe is targeted) control waveform.

The parameterized control pattern which reduces a sidelobe at a given sidelobe angle (θ_1, ϕ_1) is a renormalization of the weighted sum of the original control pattern and the auxiliary control pattern

$$\begin{aligned} m_{\mathrm{sum}}(\mathbf{r}_n; \theta_0, \phi_0) &= \cos((\mathbf{k}_s - \mathbf{k}_f(\theta_0, \phi_0)) \cdot \mathbf{r}_n) \\ &+ \alpha_1 \cos((\mathbf{k}_s - \mathbf{k}_f(\theta_1, \phi_1)) \cdot \mathbf{r}_n + \varphi_1) \end{aligned} \quad (7)$$

Then, m_{sum} is normalized to a parametric value such that $0 \le m_{\mathrm{sum}} \le 1$ for all $\mathbf{r}_n$.

This parametric value is implemented in control on the elements of the antenna as indicated in Section III-B. Note that, there are two parameters in addition to the scan angle (θ_m, ϕ_m) for each of the M auxiliary cosine waveform control patterns that are added to the base modulation pattern to target each of the M sidelobes of interest.

The two parameters to be optimized are a linear weight, α_m, and a phase-offset, φ_m, of the auxiliary waveform, see steps 5 and 6 of Fig. 2. The phase-offset must be correctly defined such that the newly produced lobe is $180°$ out of phase with the original sidelobe, while the weight must be selected to sufficiently reduce the sidelobe.

We numerically investigated the parametric geometry for a simulated 260 cell single-strip antenna when maximal reduction of the targeted sidelobe is the optimization criteria. This DDA model simulated antenna consists of a single row of meta-atom resonators fed by a single rectangular waveguide channel propagating a TE_{10} mode. The simulated array consists of a total of 260 meta-atom resonators spaced at $\lambda/5$, and simulations were performed at 30 GHz, which is above
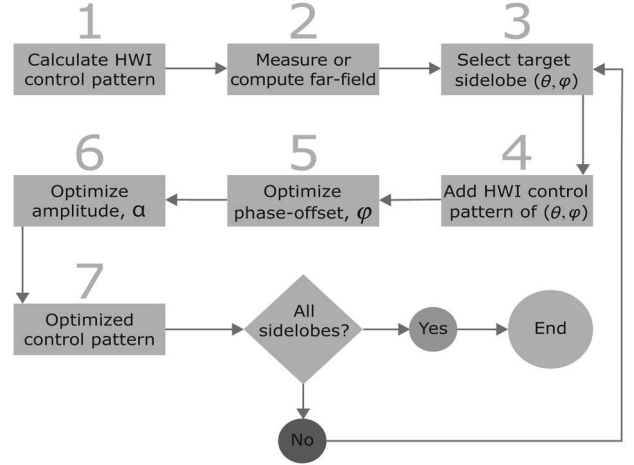

Fig. 2. Flowchart of sidelobe reduction algorithm. HWI stands for holographic wave interference, see equation 3.
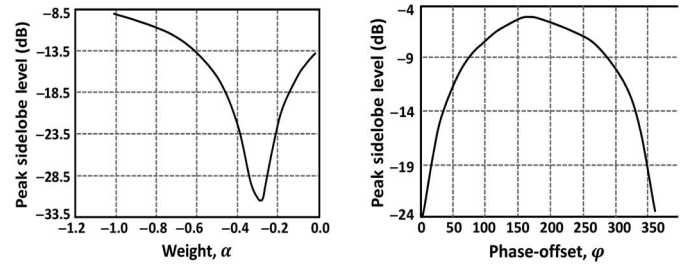

Fig. 3. Sidelobe level as a function of (left) amplitude of auxiliary pattern and (right) phase-offset of auxiliary pattern for the example of an array pointing at $-30°$ and targeting a sidelobe at $+4°$.

the upper resonance of all unit cells. The resonators possess a tuning bandwidth of 10%. We found that the control pattern parameter space is smooth with respect to each parameter independently. That is, fixing ones parameter, the sidelobe level varies smoothly with the second parameter. Fig. 3 shows two representative curves. The left image of Fig. 3 shows the sidelobe level when the phase-offset of the auxiliary pattern is fixed (at $2°$) and the weight is varied from 0 to -1; the sidelobe level varies smoothly and has a single minimum. Similarly, the right plot of the figure shows smooth variation of the sidelobe level when the weight of the auxiliary pattern is fixed at -0.27, and the phase is varied through all $360°$.

The phase and weight are well-behaved and could be defined analytically if it were true that both the *simulated, ideal* system, and *fabricated* system had linear physics. However, there are many levels at which nonlinearities are introduced both in theory and practice from build tolerances (fabrication), inexact characterization (fabrication), inexact modeling (simulation), complex coupled interactions (simulation and fabrication), and, most importantly, the application of the controls themselves (simulation and fabrication). So, it is not to be expected that linear superposition of the two patterns should work for sidelobe canceling. It is also not to be expected that the cancelation of a sidelobe should leave the rest of the pattern unaffected or the main beam intact.

In the face of the inability to know *a priori* what the optimal sidelobe-reduced pattern should be, we use a backtracking line search in conjunction with a gradient descent method to iteratively optimize one parameter at-a-time. We investigated alternating optimization of the two parameters to obtain a "simultaneously" optimized result.

However, such an algorithm converged with a greater number of iterations, making it less attractive.

It is difficult to compare the complexity or the time-to-optimization of this algorithm to other works for two reasons. First, as noted before, no other work has addressed *software control* of a reconfigurable meta-material antenna. Second, we may look to compare with phased array optimization techniques in which they seek to assign optimal weights (amplitude, phase, or both) for main beam scan and sidelobe control. This literature encompasses a wide variety of methods including both parametric and nonparametric methods [24]–[26]. However, the fact that the meta-atoms are resonant, and the response to the control is complex means that even if we knew exactly what phase and amplitude we desired, we still have the problem of finding the control which affects that desired distribution. These are problems of both the simulated antenna and the fabricated antennas, which points us, once more, toward developing an *algorithm*. To develop and test the algorithm, we employ the DDA model of the antenna, and then we use the algorithm rather than the model-optimized control values on a fabricated device. This approach permits each individual device to improve its own pattern in spite of variations. The method presented here is of particular value because it guarantees reduction of any targeted sidelobe, learning optimal controls for whole antennas in the presence complete, complex, manufactured-antenna physics.

V. RESULTS

Results are presented here from using the *algorithm* of Section IV both on a simulated antenna and on a fabricated device. That is, the entire algorithm is applied in each scenario rather than using the algorithm to optimize in simulation and then transcribing control values to the device. These results show the ability of the algorithm to iteratively and significantly reduce undesired sidelobes while not degrading the rest of the far-field pattern.

Fig. 1(d) shows iterative sidelobe targeting for the simulated 260-cell 30 GHz single-strip antenna simulated with a DDA model (the same antenna model described in the previous section). The main beam points to $25.7°$ θ, and the algorithm reduces 5 sidelobes at $-31.1°$, $-62.0°$, $-64.6°$, $-27.9°$, and $-60.3°$, in order. It reduces each of these sidelobes by 17.62, 3.98, 4.43, 8.92, and 1.87 dB, respectively. The algorithm successfully reduces the original pattern whose first sidelobe was only 8 dB down from the main beam, and produces a pattern where all sidelobes are more than 22 dB down.

Fig. 1(d) also shows a physical representation of what these antenna patterns mean in a mobile use-case. The antenna is placed on the top of a vehicle, and the arrows show where the primary energies of the antenna are pointing. As the algorithm progresses, the sidelobes shrink rapidly until we are left mostly with just a main beam in the desired direction. The antenna is no longer at risk of interfering with other satellites' transmissions nor at risk of receiving unacceptable levels of noise.

The pattern after running the algorithm to cancel sidelobes, as one might anticipate from the intentional distortion of the ideal single-tone cosine wave control, will suffer a small reduction in peak gain. This is intuitively understood, since small amounts of the radiated energy are being directed away from the main beam to point in the direction of the sidelobe. However, this reduction has been seen in experiment to be slight in comparison to the large drop in sidelobe amplitude since the original control waveform will still dominate, (see Fig. 4). Fig. 4 shows the gain reduction as a function of the number of sidelobes killed-off for several trials of the algorithm on the DDA-modeled antenna strip. The gain drops significantly with the first targeted sidelobe and then degrades more slowly as further sidelobes are targeted. This is largely due to the fact that the first sidelobe targeted is the largest,
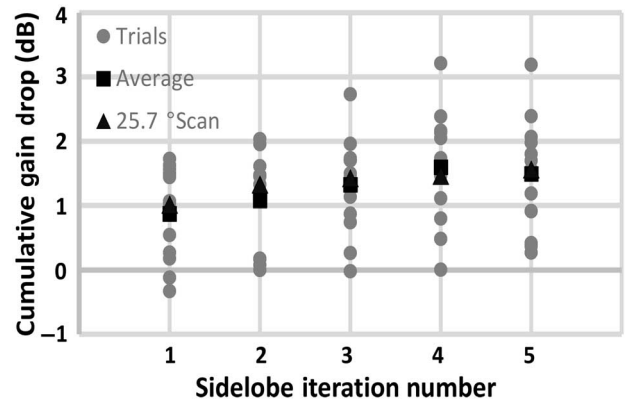

Fig. 4. (a) Cumulative reduction in gain (dB) as a function of the number of targeted sidelobes over 13 trials at equally spaced scan angles between $-30°$ θ and $+30°$ θ with the average reduction (square) and the reduction for the scan angle $25.7°$ with complete results shown in Fig. 1(d).

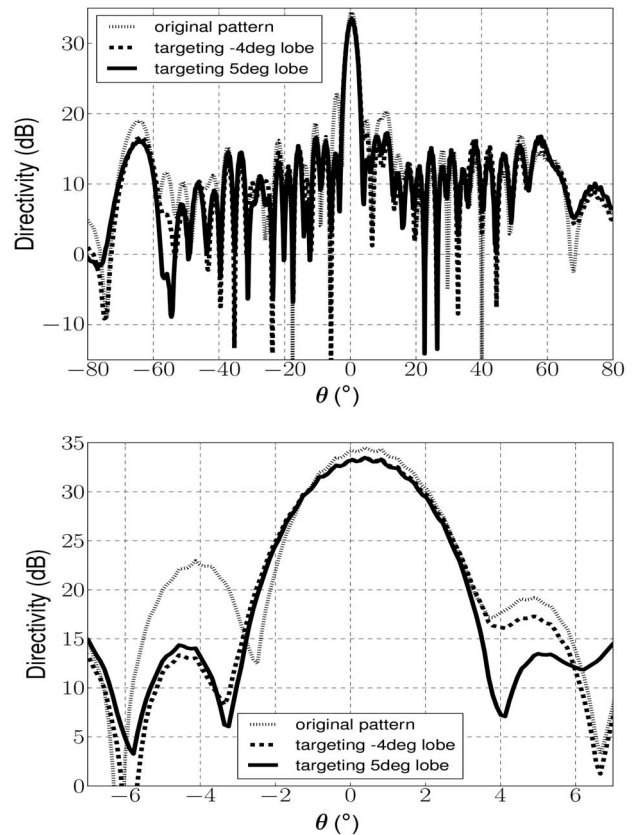
Fig. 5. Measured results from a 96-cell single-channel aperture. The aperture controlled to point to $0°$ θ (broadside) and the algorithm was used to reduce the first two sidelobes at $-4°$ (by ≈ 8 dB) and $+5°$ degrees (by ≈ 6 dB). (Top) Entire visible angular region and (bottom) enlargement of the main beam and targeted sidelobe region.

and the weight α which is optimal to reduce this sidelobe is much larger than the weight necessary for a smaller sidelobe. Thus, with the first, large sidelobe, the auxiliary pattern skews the primary pattern much more heavily than any subsequent addition. Note, however, that the gain reduction is significantly less than the improvement in the sidelobe level.

Importantly, Fig. 5 shows the results of using this algorithm on a fabricated antenna to iteratively develop a control pattern that yields

an improved far-field pattern. This antenna is an even smaller single-strip prototype. This antenna has only 96 cells, but possess the same operating characteristics, namely, operation at 30 GHz equally spaced cells at $\lambda/5$ and an individual resonator tuning bandwidth of 10%. The antenna is commanded to scan to broadside ($0°$ θ), and the first two sidelobes, first $-4°$ and then $+5°$, are reduced with the cancelation algorithm. The $-4°$ sidelobe was reduced by approximately 8 dB, and the $+5°$ sidelobe was reduced by approximately 6 dB. Note that, the rest of the pattern is relatively unperturbed, and in some place is noticeably improved even though those sidelobes were not targeted. Also note that, after the $-4°$ lobe is targeted, the $+5°$ sidelobe correction did not degrade, the $-4°$ sidelobe improvement by much. Since the modulation patterns are independent, they only effect specific spatial points.

VI. Conclusion

This paper addresses sidelobe cancelation for the optimization of the radiated far-field pattern of a holographic metamaterial antenna. This paper is a first work on the topic: providing an efficient and robust algorithm for optimizing performance of an MSA. An algorithm to reduce sidelobes was introduced and was successfully demonstrated for both the modeled system and in experiment.

There are several directions to extend this work including exploring methods for full planar aperture optimization. First, the algorithm could be immediately applied on a full aperture as implemented on the single channel, adding the complete 2-D wave interference control pattern of a sidelobe to all the channels of the aperture, simultaneously. This would maintain exactly the same complexity as the 1-D case (two additional parameters for every sidelobe targeted). However, a second approach would be to attempt to exploit adjacent rows for cancellation of sidelobes introduced by other neighboring rows. This could prevent main beam gain degradation, but would introduce complexity that scales linearly with the number of channels.

Perhaps, of the greatest interest, however, is using this optimization algorithm for real-time control and adaptation in the field, appropriately using modeled predictions and feedback from the antenna's sensors, and the satellite communications hub to optimize the pattern on-the-fly. Modeled results along with historical data could be used to provide excellent starting points for the optimization with feedback from the hub allowing for live updating and optimization of the control pattern.

References

[1] G. Lipworth *et al.*, "Metamaterial apertures for coherent computational imaging on the physical layer," *J. Opt. Soc. Amer. A*, vol. 30, pp. 1603–1612, 2013.

[2] S. Lim, C. Caloz, and T. Itoh, "Metamaterial-based electronically controlled transmission-line structure as a novel leaky-wave antenna with tunable radiation angle and beamwidth," *IEEE Trans. Microw. Theory Techn.*, vol. 52, no. 12, pp. 2678–2690, Dec. 2004.

[3] K. M. Palmer, "Metamaterials make for a broadband breakthrough," *IEEE Spectr.*, vol. 49, no. 1, pp. 13–14, Jan. 2012.

[4] P. W. Howelss, "Intermediate frequency side-lobe canceller," U.S. Patent 3 202 990, Aug. 24, 1965.

[5] D. D. Howard, "Sidelobe cancelling system for array type target detectors," U.S. Patent 3 435 453, Mar. 25, 1969.

[6] I. Durboraw, "Clutter compensated sidelobe cancelling communications system," U.S. Patent 4 381 508, Apr. 26, 1983.

[7] I. Tsujimoto, "Sidelobe cancellation and diversity reception using a single array of auxiliary antennas," U.S. Patent 5 369 412, Nov. 29, 1994.

[8] C. Baird and G. Rassweiler, "Adaptive sidelobe nulling using digitally controlled phase-shifters," *IEEE Trans. Antennas Propag.*, vol. 24, no. 5, pp. 638–649, Sep. 1976.

[9] L. J. Griffiths and C. W. Jim, "An alternative approach to linearly constrained adaptive beamforming," *IEEE Trans. Antennas Propag.*, vol. 30, no. 1, pp. 27–34, Jan. 1982.

[10] W. Herbordt and W. Kellermann, "Efficient frequency-domain realization of robust generalized sidelobe cancellers," in *Proc. IEEE Workshop Multimedia Signal Process.*, 2001, pp. 377–382.

[11] B. Widrow *et al.*, "Adaptive noise cancelling: Principles and applications," *Proc. IEEE*, vol. 63, no. 12, pp. 1692–1716, Dec. 1975.

[12] P. Checcacci, V. Russo, and A. Scheggi, "Holographic antennas," *IEEE Trans. Antennas Propag.*, vol. 18, no. 6, pp. 811–813, Nov. 1970.

[13] B. H. Fong, J. S. Colburn, J. J. Ottusch, J. L. Visher, and D. F. Sievenpiper, "Scalar and tensor holographic artificial impedance surfaces," *IEEE Trans. Antennas Propag.*, vol. 58, no. 10, pp. 3212–3221, Oct. 2010.

[14] G. Minatti, F. Caminita, M. Casaletti, and S. Maci, "Spiral leaky-wave antennas based on modulated surface impedance," *IEEE Trans. Antennas Propag.*, vol. 59, no. 12, pp. 4436–4444, Dec. 2011.

[15] G. Minatti, S. Maci, P. De Vita, A. Freni, and M. Sabbadini, "A circularly-polarized isoflux antenna based on anisotropic metasurface," *IEEE Trans. Antennas Propag.*, vol. 60, no. 11, pp. 4998–5009, Nov. 2012.

[16] S. K. Podilchak, L. Matekovits, A. P. Freundorfer, Y. M. M. Antar, and M. Orefice, "Controlled leaky wave radiation from a planar configuration of width-modulated microstrip lines," *IEEE Trans. Antennas Propag.*, vol. 61, no. 10, pp. 4957–4972, Oct. 2013.

[17] G. Taylor *et al.*, "Reconfigurable antenna," U.S. Patent 6 567 046, May 20, 2003.

[18] D. Sievenpiper *et al.*, "A tunable impedance surface performing as a reconfigurable beam steering reflector," *IEEE Trans. Antennas Propag.*, vol. 50, no. 3, pp. 384–390, Mar. 2002.

[19] F. Costa, A. Monorchio, S. Talarico, and F. M. Valeri, "An active high-impedance surface for low-profile tunable and steerable antennas," *IEEE Antennas Wireless Propag. Lett.*, vol. 7, pp. 676–680, Jan. 2009.

[20] D. J. Gregoire, J. S. Colburn, A. M. Patel, R. Quarfoth, and D. F. Sievenpiper, "A low profile electronically-steerable artificial-impedance-surface antenna," in *Proc. Int. Conf. Electromagn. Adv. Appl. (ICEAA'14)*, 2014, pp. 477–479.

[21] L. Matekovits, M. Heimlich, and K. Esselle, "Metamaterial-based millimeter-wave switchable leaky wave antennas for on-chip implementation in GaAs technology," *J. Electromagn. Waves Appl.*, vol. 25, no. 1, pp. 49–61, 2011.

[22] L. Matekovits, M. Heimlich, and K. P. Esselle, "Tunable periodic microstrip structure on GaAs wafer," *Prog. Electromagn. Res.*, vol. 97, pp. 1–10, 2009.

[23] M. C. Johnson, P. T. Bowen, N. Kundtz, and A. Bily, "A discrete-dipole approximation model for control and optimization of a holographic metamaterial antenna," *Appl. Opt.*, vol. 53, no. 25, pp. 5791–5799, 2014.

[24] A. K. Bhattacharyya, *Phased Array Antennas: Floquet Analysis, Synthesis, BFNs and Active Array Systems*, vol. 179. Hoboken, NJ, USA: Wiley, 2006.

[25] R. J. Mailloux, *Phased Array Antenna Handbook*. Norwood, MA, USA: Artech House, 2005.

[26] R. C. Hansen, *Phased Array Antennas*, vol. 213. Hoboken, NJ, USA: Wiley, 2009.